Received November 24, 2014, accepted December 22, 2014, date of publication February 19, 2015, date of current version May 21, 2015.

Digital Object Identifier 10.1109/ACCESS.2015.2404812

Reliability and Failure Modes of Solid-State Lighting Electrical Drivers Subjected to Accelerated Aging

PRADEEP LALL[1], (Fellow, IEEE), PETER SAKALAUKUS[1], (Member, IEEE), AND LYNN DAVIS[2]
[1]NSF-CAVE3 Electronics Research Center, Department of Mechanical Engineering, Auburn University, Auburn, AL 36849 USA
[2]RTI International, Durham, NC 27709 USA

Corresponding author: P. Lall (lall@auburn.edu)

The work was supported by the National Renewable Energy Laboratory, Office of Energy Efficiency and Renewable Energy through the U.S. Department of Energy under Award DE-EE0005124.

ABSTRACT An investigation of an off-the-shelf solid-state lighting device with the primary focus on the accompanied light-emitting diode (LED) electrical driver (ED) has been conducted. A set of 10 EDs were exposed to temperature humidity life testing of 85% RH and 85 °C (85/85) without an electrical bias per the JEDEC standard JESD22-A101C in order to accelerate the ingress of moisture into the aluminum electrolytic capacitor (AEC) and the EDs in order to assess the reliability of the LED drivers for harsh environment applications. The capacitance and equivalent series resistance for each AEC inside the ED were measured using a handheld *LCR* meter as possible leading indications of failure. The photometric quantities of a single pristine light engine were monitored in order to investigate the interaction between the light engine and the EDs. These parameters were used in assessing the overall reliability of the EDs. In addition, a comparative analysis has been conducted between the 85/85 accelerated test data and a previously published high-temperature storage life accelerated test of 135 °C. The results of the 85/85 acceleration test and the comparative analysis are presented in this paper.

INDEX TERMS Electrolytic capacitor, solid-state lighting, LED.

I. MOTIVATION

The U.S. Department of Energy has made a long-term commitment to advance R&D breakthroughs in efficiency and performance of SSL technology [1] due to the passing of the Energy Independence and Security Act of 2007 (EISA) [2]. Additionally, AECs are traditionally the weakest link inside LED drivers making them a desirable candidate for the prognostication of LED ED failure [3]. Lastly, there is a lack of published accelerated test methods for SSL devices to assess reliability, as well as a need for physics based prognostic indicators for the assessment and prediction of SSL life.

II. INTRODUCTION

Today's lighting technology is steadily becoming more energy efficient and less toxic to the environment since the passing of the EISA. EISA has mandated a higher energy efficiency standard for lighting products and the phase out of the common incandescent light bulb. This has led lighting manufacturers to pursue SSL technologies for consumer lighting applications. However, two major roadblocks are hindering the transition process to SSL luminaires: cost and quality. In order to cut cost, manufactures are moving towards cheaper packaging materials and a variety of package architecture construction techniques which may potentially erode the quality of the luminaire and reduce its survivability in everyday applications, such as automotive, aerospace and marine. SSL devices are being introduced as headlamps in some of today's luxury automobiles and may also be fulfilling a variety of important outdoor applications such as overhead street lamps, traffic signals and landscape lighting. SSL devices in these environments are almost certain to encounter excessive moisture ingress from humidity and high temperatures for a persistent period of time.

The SSL package architecture must be designed with performance factors in mind, as well as address some of the known and published LED related failure mechanisms, such as carbonization of the encapsulant material, delamination, encapsulant yellowing, lens cracking, and phosphor thermal quenching [4]. Each failure mechanism produces the similar failure mode of lumen degradation predominately due to

2169-3536 © 2015 IEEE. Translations and content mining are permitted for academic research only.
Personal use is also permitted, but republication/redistribution requires IEEE permission.
See http://www.ieee.org/publications_standards/publications/rights/index.html for more information.

two contributing factors: high junction temperature and moisture ingress. The current state-of-the-art has focused on individual areas of the SSL light engine design, such as the LED chip, substrate material and thermal management techniques with a minimal investigation on the reliability and performance of LED EDs [5]–[16]. This work has focused on expanding the understanding of LED EDs by investigating the degradation in the AECs as possible prognostic indicators of failure well before failure occurs.

AECs have the highest failure rates compared to the other components that compromise an ED and are considered the ''weakest-link'' [17]–[20]. AEC degradation may cause the EDs to fail completely due to a current surge or produce an undesirable light output of the LED array. An AEC is a type of capacitor that uses an electrolyte to achieve a larger capacitance per unit volume compared to traditional capacitors. They are used in high current and low frequency electrical circuits, such as an LED electrical driver, and are needed to help convert AC power to DC power [21]. An AEC is composed of a cathode aluminum foil, electrolytic paper, liquid electrolyte and a dielectric [22], [23]. The capacitance can be calculated by knowing the dielectric constant, surface area of the dielectric and the thickness of the dielectric [22]–[24]. The ESR can be found by summing the electrolytic resistance, dielectric loss and the electrode resistance using equations outlined in the literature [22], [25], and [26]. In this work, the ESR and CAP were measured using a handheld LCR meter instead of estimating the parameters needed to determine suitable CAP and ESR values.

The predominant failure mechanism of the AEC is the loss of the liquid electrolyte through dissipation and decomposition. Liquid electrolyte loss can be attributed to an elevated ambient temperature, electrochemical reactions at the dielectric layer, moisture ingress or diffusion through the seal [24], [25]. This will lead to a drift of the electrical parameters of the AEC (i.e. CAP and ESR). If an AEC is kept at an elevated ambient temperature for a prolonged period of time causing liquid electrolyte degradation, then the capacitance will decrease and the ESR will increase [22]–[33]. Literature has shown that CAP and ESR are excellent leading indications of failure for prognostic and health management techniques [17]–[19], as well suitable parameters to investigate LED driver reliability [20].

Therefore, CAP and ESR are excellent candidates to monitor the overall health of the ED in the pre-failure space. This along with the photometric output of the pristine light engine gives great insight into the interaction between the light engine and the ED. The results of the ESR and CAP measurements for the AECs subjected to 85/85 (JESD22-A101C [34]) testing are presented in this work. The photometric parameters of the single pristine light engine with the EDs under test were determined using the IES LM-79-08 testing standards to investigate changes in the output of the ED [35]. The failure sites, as well as the failure modes of the EDs have been determined and are presented in this paper. Additionally, a comparative analysis has been conducted between the 85/85 accelerated test data and a previously published high temperature storage life accelerated test of 135°C (HTSL) [5].

III. PHOTOMETRIC THEORY

The IES LM-79-08 standard states that the total spectral radiant flux, $\Phi_{test}(\lambda)$, of a SSL product under test can be obtained by comparison to a known reference or calibration standard, $\Phi_{ref}(\lambda)$, spectral radiant flux [35]. It is determined using (1) where $y_{test}(\lambda)$ and $y_{ref}(\lambda)$ are the spectrometer readings of the lamp under test and the reference lamp found using the integrating sphere, respectively.

$$\Phi_{test}(\lambda) = \left[\Phi_{ref}(\lambda) \cdot \frac{y_{test}(\lambda)}{y_{ref}(\lambda)}\right] \cdot \alpha_{CCF} = \Phi_m(\lambda) \cdot \alpha_{CCF}$$
$$\alpha_{CCF}(\lambda) = \frac{y_{aux,REF}(\lambda)}{y_{aux,TEST}(\lambda)} \quad (1)$$

Once the integrating sphere has been calibrated with the known calibration standard, the bracketed term in (1) is calculated internally by the SpectraSuite software with the measured spectral radiant flux, $\Phi_m(\lambda)$, of the test lamp becoming the output of the software. The self-absorption factor, α_{CCF}, can be found through a comparison of an auxiliary lamp measurement with the test lamp inside the integrating sphere, $y_{aux,Test}(\lambda)$, and an auxiliary lamp measurement with the calibration lamp standard inside the sphere, $y_{aux,REF}(\lambda)$ [35]. Both the test lamp and calibration lamp standard are off during the auxiliary measurements. The self-absorption factor is a critical parameter since SSL products typically have a different physical size, shape and absorption characteristics when compared to the calibration lamp standard used to calibrate the integrating sphere and the spectrometer. The total luminous flux, Φ_{test}, in lumens [lm] of the SSL product under test can now be found using the total spectral radiant flux found from (1) with (2) [35].

$$\Phi_{test} = K_m \cdot \int_{380}^{780} \Phi_{test}(\lambda) \cdot V(\lambda) \cdot d\lambda$$
$$K_m = 683 lm/W \quad (2)$$

The spectral luminous efficiency function for photopic vision, $V(\lambda)$, is well documented in literature and K_m is the maximum spectral luminous efficacy [36].

The tristimulus values for the lamp under test are computed using the spectral radiant flux obtained from (1) and the CIE 1931 color matching functions from a standard 2° observer [36]–[38].

$$X = k \cdot \int_{380}^{780} \Phi_{test}(\lambda) \cdot \bar{x}(\lambda) \cdot d\lambda$$
$$Y = k \cdot \int_{380}^{780} \Phi_{test}(\lambda) \cdot \bar{y}(\lambda) \cdot d\lambda$$
$$Z = k \cdot \int_{380}^{780} \Phi_{test}(\lambda) \cdot \bar{z}(\lambda) \cdot d\lambda \quad (3)$$

IEEE Access
The journal for rapid open access publishing

The color matching functions ($\bar{x}(\lambda)$, $\bar{y}(\lambda)$ and $\bar{z}(\lambda)$) are provided with seven significant figures by the CIE in tabular form at 1nm intervals over the visible light spectrum [38]. The variable k is known as the normalizing factor and is shown in (4) [37], [38].

$$k = \frac{100}{\int_{380}^{780} E(\lambda) \cdot \bar{y}(\lambda) \cdot d\lambda} \tag{4}$$

In this equation, E(λ) is the relative spectral power distribution of a CIE standard illuminant. For this work, the CIE standard illuminant A was chosen. Once the Tristimulus values are obtained, the CIE 1931 color space coordinate system can be calculated [36]–[38].

$$x = \frac{X}{X+Y+Z}$$
$$y = \frac{Y}{X+Y+Z} \tag{5}$$

The coordinate system is then transformed to the CIE 1976 color space because the chromaticity of this space is more uniform than the CIE 1931 color space [39].

$$u` = \frac{2x}{6y - x + 1.5}$$
$$v` = \frac{4.5y}{6y - x + 1.5} \tag{6}$$

The correlated color temperature (CCT) of a luminaire under test is the temperature of an ideal black-body radiator with a comparable hue. The isotemperature line that denotes the CCT of the luminaire is perpendicular to the Planckian locus and can be approximated with a high degree of certainty using the third-power polynomial shown below [39], [40].

$$CCT_{PL} = 437n^3 + 3601n^2 + 6831n + 5517$$
$$n = \frac{x - 0.332}{0.185 - y} \tag{7}$$

Equation (7) produces two complex numbers and one real number. Therefore, the real solution is the correct choice for the CCT [39], [40].

IV. TEST VEHICLE

The test vehicle for this work was an off-the-shelf SSL device which consisted of a LED downlight module, an electrical driver (boost PWM half-bridge rectifier) and wired connections to attach the two components, as well as to connect the electrical driver to the main power supply. A single pristine light engine was used in this experiment with a set of ten EDs used to power the light engine as described below. This approach facilitates assignment of any observed changes in lumen maintenance caused by the degradation of the EDs. Fig. 1 illustrates how each component of the system is incorporated. A base line luminous flux value was obtained using an untested electrical driver during each time step. The pristine value was used as a comparison to the luminous flux values found for each ED under 85/85 in order to investigate minute changes in the lumen maintenance.

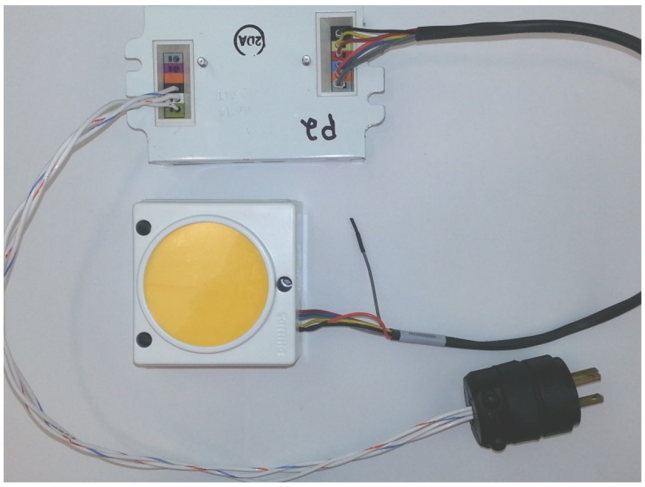

FIGURE 1. The SSL electrical driver and light engine used in this experimental work.

Ten sample sets consisting of four AECs each were used in this experiment. Each sample set was taken from a separate, single ED. These AECs were removed to in order to measure the CAP and ESR. Fig. 2 depicts the circuit board of a single electrical driver with the four AECs removed.

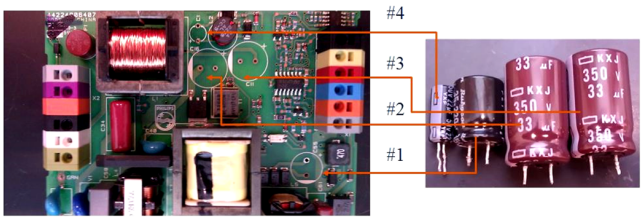

FIGURE 2. The removed AECs and their corresponding location inside the electrical drivers subjected to 85/85.

Each electrical driver consisted of four AECs of three different types. The useful AEC characteristics are given in Table 1.

TABLE 1. Parameters for each AEC.

AEC #	Endurance [Hrs]	T_o [°C]	V_o [Vdc]	C_o [μF]
1	8000 to 10000	-40 to +105	35	220
2	10000 to 12000	-40 to +105	350	33
3	10000 to 12000	-40 to +105	350	33
4	4000 to 5000	-40 to +105	50	22

V. TEST ENVIRONMENT

The removed AECs and the remaining portion of the electrical driver were kept in a Thermotron humidity chamber at 85/85 for the duration of the test. Once the components were removed from the chamber, they were allowed to cool to room temperature for approximately one hour before measurements were taken. The ESR and CAP of each AEC

were measured directly using an Agilent U1733C handheld LCR meter.

Photometric calculations were also carried out for each ED and the pristine light engine following the IES LM-79-08 standard [35]. The AECs were connected to its corresponding ED through a bread board. The light output leads of the ED were connected to another portion of the bread board which allowed easy switching between EDs to record the radiant flux as a function of wavelength. The measurements were conducted at room temperature. An USB4000 Spectrometer from Ocean Optics, SpectraSuite software and a one meter integrating sphere were used to accurately obtain the radiant flux data of the light engine for each ED. The radiant flux was used to determine the luminous flux, chromaticity coordinates, color shift and the correlated color temperature. Fig. 3 illustrates the luminous flux setup.

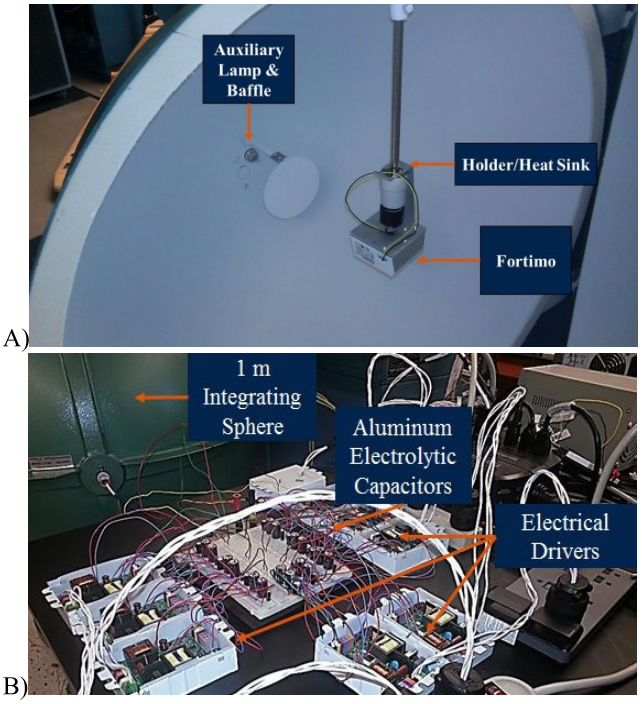

FIGURE 3. Luminous flux measurement setup: A) inside the integrating sphere and B) outside the integrating sphere.

VI. EXPERIMENTAL RESULTS

In this work, 85/85 testing was conducted on a sample set of ten EDs until complete failure was reached. The CAP and ESR of the AECs were measured at regular intervals, as well as the luminous flux of the pristine light engine using each ED. The luminous flux for each ED never deviated outside of the pristine range given by the manufacturer through the course of the experiment. Luminous flux gave no indication of possible degradation inside the EDs. Therefore, it was not a suitable indicator to describe the degradation of the EDs under 85/85 testing. Each ED was tested until a failure mechanism was present with the last failure occurring at 4294.4 hours. Fig. 4 shows the relative luminous flux values (measured value divided by original value) over the course of 85/85 accelerated testing for all ten EDs.

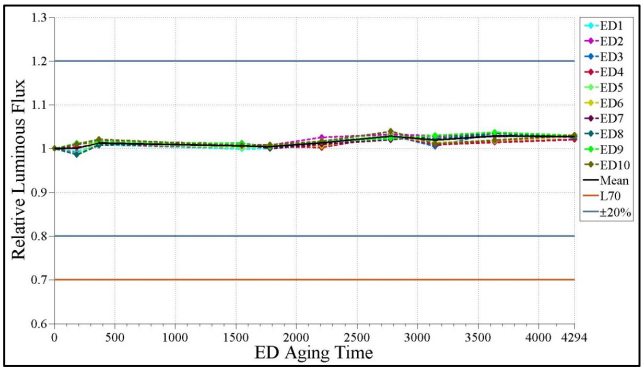

FIGURE 4. The relative luminous flux of the pristine light engine using each ED subjected to 85/85.

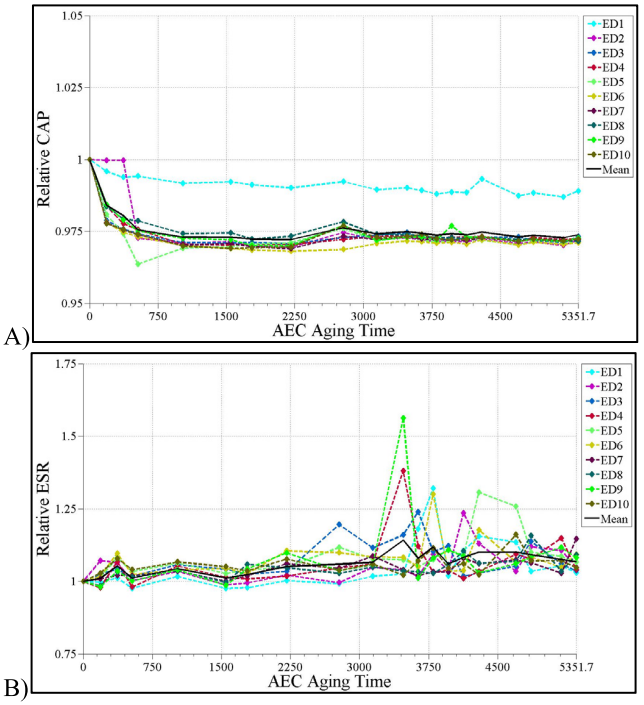

FIGURE 5. The relative A) CAP and B) ESR of AEC 1 from each ED subjected to 85/85.

The CAP and ESR also did not forecast the degradation of the EDs prior to failure. After failure occurred in each ED the AECs were placed back into 85/85 testing for further investigation with testing completely stopped at 5351.65 hours due to negligible change in the CAP and ESR values. Fig. 5 – Fig. 8 graphically compares the collected CAP and ESR data of each AEC from the EDs. The fluctuations in the ESR values may be attributed to measurement error or a minute amount of atmospheric corrosion occurring on the metallic leads preventing a suitable connection of the

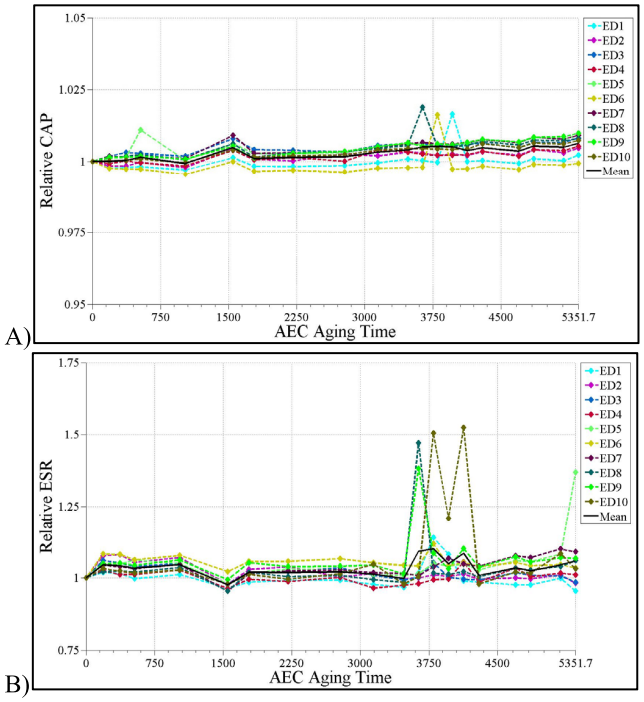

FIGURE 6. The relative A) CAP and B) ESR of AEC 2 from each ED subjected to 85/85.

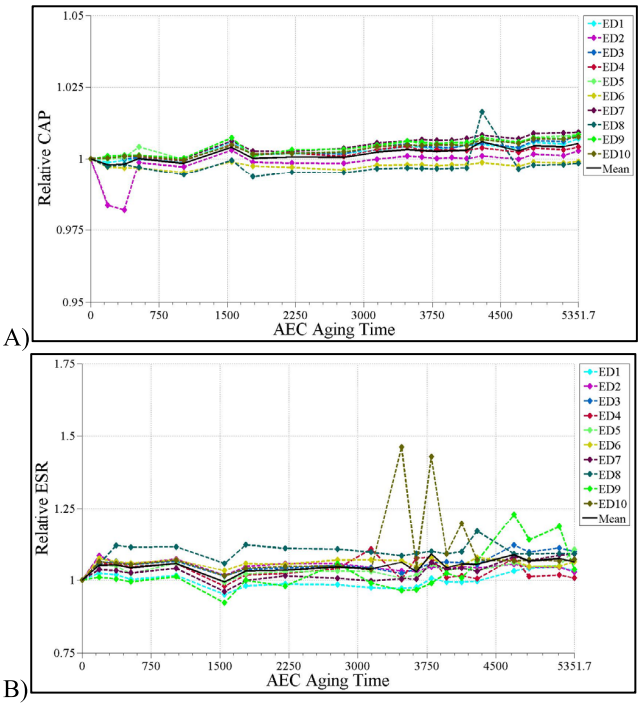

FIGURE 7. The relative A) CAP and B) ESR of AEC 3 from each ED subjected to 85/85.

measurement probes since corresponding values were closer to the actual pristine value.

Unfortunately, the hypothesis that the AEC would be the ''weakest-link'' inside the LED ED proved to be incorrect

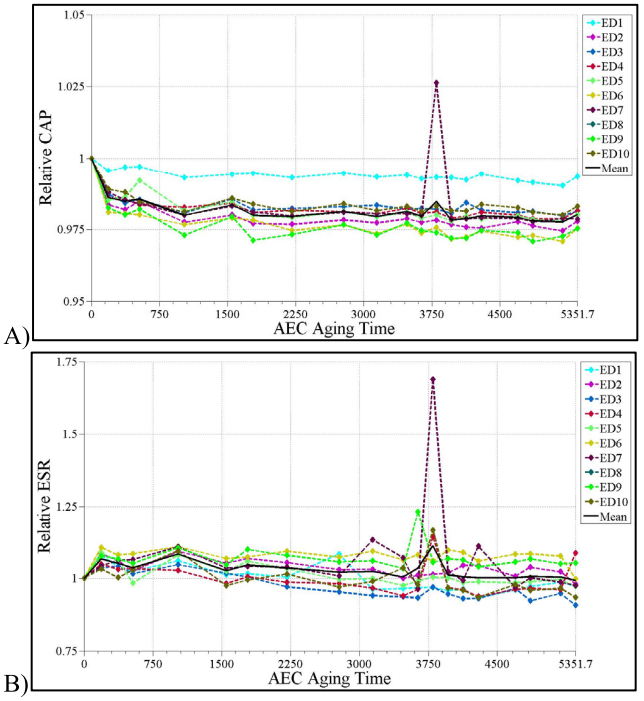

FIGURE 8. The relative A) CAP and B) ESR of AEC 4 from each ED subjected to 85/85.

TABLE 2. Failures characterization of EDs from 85/85 testing.

Driver	T_f [Hrs]	Failure Site	Failure Mode
# 1	333.37	IGBT/MOSFET	Short Circuit
# 2	0.00	Unknown	Short Circuit
# 3	3143.78	CL21-S PFCAP	CAP Leakage
# 4	3635.37	CL21-S PFCAP	CAP Leakage
# 5	0.00	SMD-R 1206	Short Circuit
# 6	3635.37	CL21-S PFCAP	CAP Leakage
# 7	369.12	IGBT/MOSFET	Short Circuit
# 8	185.15	SMD-C 1206	Short Circuit
# 9	369.12	IGBT/MOSFET	Short Circuit
# 10	3635.37	CL21-S PFCAP	CAP Leakage

for 85/85 accelerated aging. The temperature condition for this test was well below the maximum rated operating temperature for the AECs which proved too small to induce degradation in the form of electrolytic loss. Additionally, the construction of the AECs did not allow for the ingress of moisture that potentially would dilute the electrolyte producing a decrease in capacitance. However, the ten EDs did experience component level failure which rendered each electrical driver useless to some degree. Multiple failure sites have been determined with each ED experiencing only one of the failure sites. Table II catalogs the failure site and failure modes of each ED that underwent 85/85 testing.

The figure above depicts a pristine electrical driver from the top and bottom views to show the placement of each

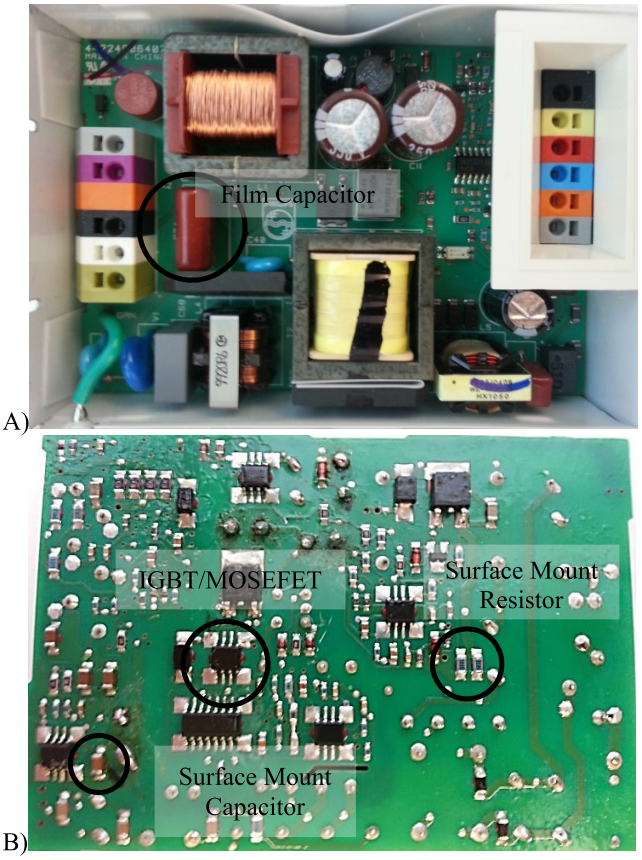

FIGURE 9. Identification of the failure site locations inside the EDs: A) top view and B) bottom view.

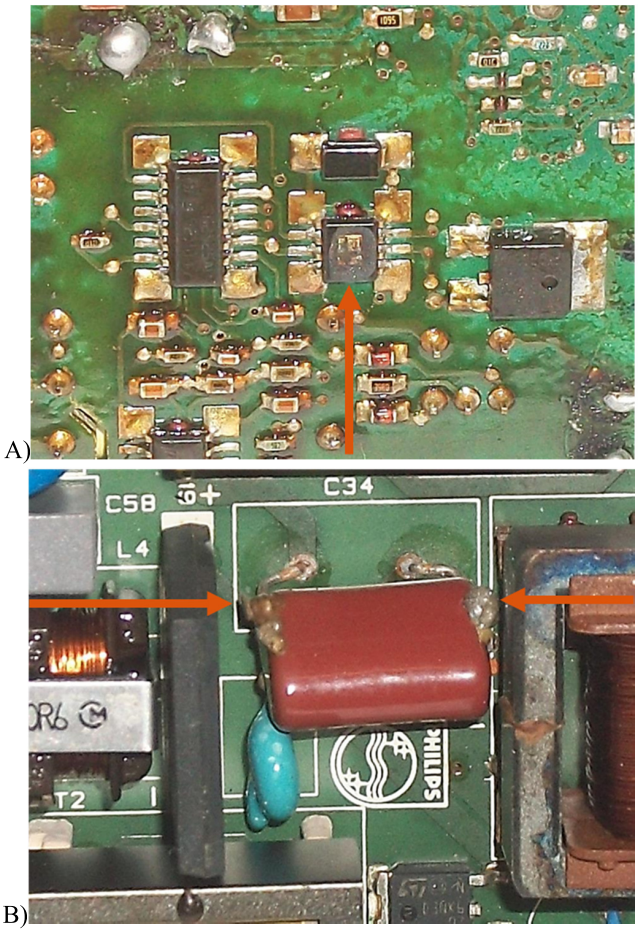

FIGURE 10. A failed A) IGBT/MOSFET and B) film capacitor inside the EDs. These predominate failure sites encompassed 70% of the EDs.

failed component. The different failure sites listed in table 2 have been circled in Figure 9 to show the components in their pristine form and their location inside the electrical driver. Optical images for each ED's failed components under 85/85 accelerated aging can be found in previously published work [41]. Figure 10 depicts the two predominate failure sites encountered during 85/85 accelerated aging: IGBT/MOSFET and the film capacitor.

Since the CAP & ESR of the AECs and the luminous flux of the lighting system did not give any sign of impending failure, additional photometric parameters were studied as possible leading indicators of failure. The CCT, CIE 1976 chromaticity color space (u` & v`) and the color shift were calculated to investigate the interaction of the LED EDs and the light engine. The results are shown below in Fig. 11 – Fig. 14 with the values of each ED plotted on the same graph.

From the graphs above, the CCT, u`-coordinate and v`-coordinate are virtually constant throughout the course of experimentation. These parameters also suggest that the system is healthy with no indication of imminent failure inside the EDs. The color shift of the light engine has a minimal to nonexistent change. As a point of reference, the DOE's 2012 color shift target of 0.007 after 6000 hours and

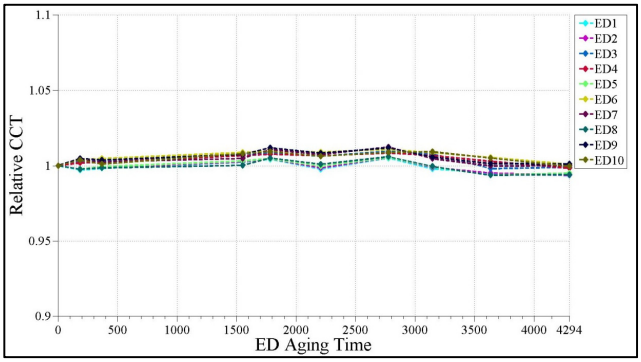

FIGURE 11. The relative CCT of the pristine light engine using each ED subjected to 85/85.

the 2020 target of 0.002 over the lifetime of the lighting system are given. The color shift for this SSL device stays below both DOE targets. Consequently, color shift did not forecast impending failure inside the EDs. From the photometric analysis, indications of catastrophic failure were not present.

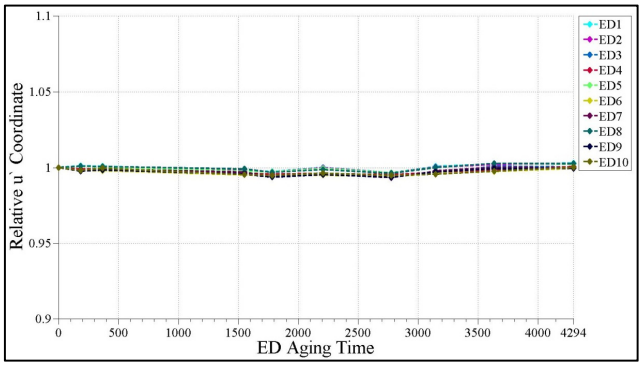

FIGURE 12. The relative u` from the CIE 1976 color space of the pristine light engine using each ED subjected to 85/85.

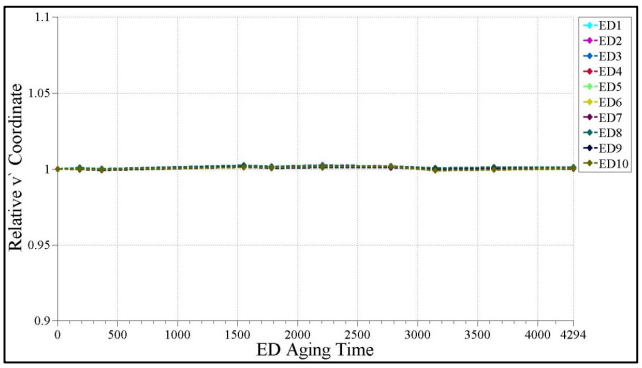

FIGURE 13. The relative v` from the CIE 1976 color space of the pristine light engine using each ED subjected to 85/85.

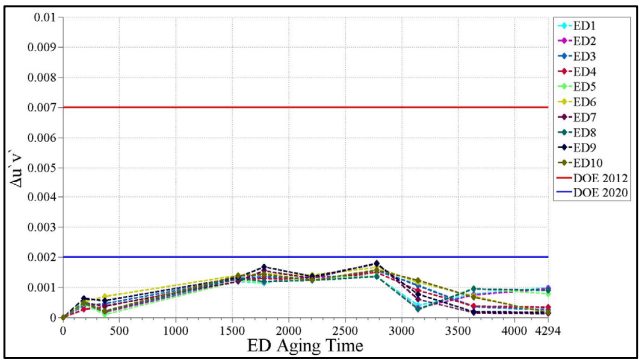

FIGURE 14. The CIE 1976 coordinate system color shift of the pristine light engine using each ED subjected to 85/85.

Since the photometric analysis for 85/85 was inconclusive, a statistical analysis of the photometric quantities was conducted to show that the ESR and CAP results of the 85/85 test and a previously reported HTSL test can be compared. HTSL testing was used to investigate the effects of time and temperature on the AECs and EDs for thermally activated failure mechanisms conducted under storage conditions, i.e. no electrical bias [42]. Fig. 15 and Fig. 16 illustrate the univariate distribution of the initial luminous flux and CCT, respectively, as well as the statistical parameters of initial luminous flux and CCT in Table 3 and Table 4, respectively.

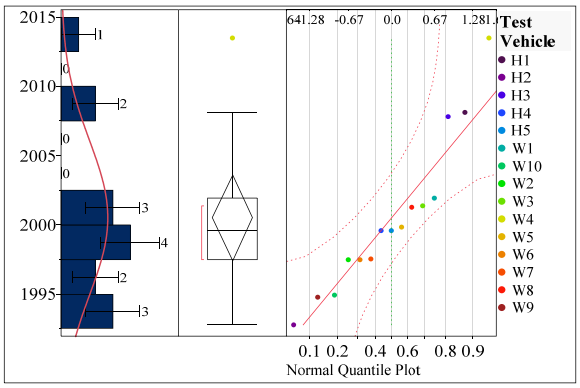

FIGURE 15. The initial luminous flux [lm] of the pristine light engine using each ED subjected to 85/85.

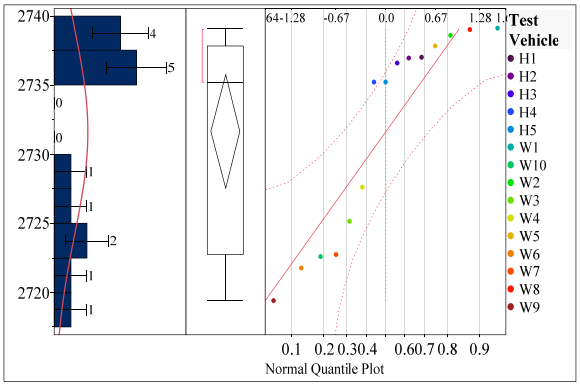

FIGURE 16. The initial CCT [K] of the pristine light engine using each ED subjected to 85/85.

TABLE 3. Statistical parameters for Figure 15.

Mean (lm)	2000.5347
Standard Deviation (lm)	5.580083
Standard Error of the Mean (lm)	1.4407712
Upper 95% Mean (lm)	2003.6248

TABLE 4. Statistical parameters for Figure 16.

Mean [K]	2731.6552
Standard Deviation [K]	7.4069642
Standard Error of the Mean [K]	1.9124699
Upper 95% Mean [K]	2735.757

TABLE 5. Statistical parameters for Figure 17.

Mean	1.0000468
Standard Deviation	0.0076458
Standard Error of the Mean	0.0020434
Upper 95% Mean	1.0044613

The rated luminous flux and CCT values for this SSL device are 2000lm ± 10% and 2700K, respectively. From the univariate distribution of the initial luminous flux,

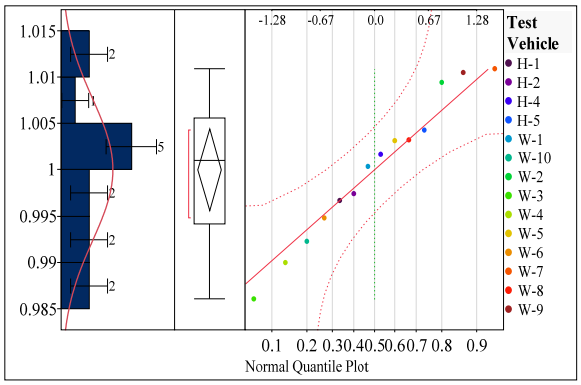

FIGURE 17. The normalized luminous flux of the pristine light engine using each ED subjected to 85/85 at 3154 hours.

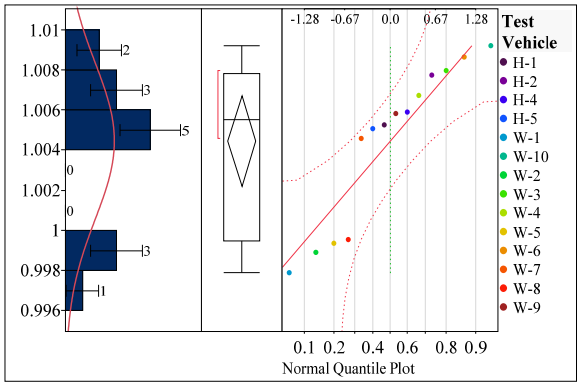

FIGURE 18. The normalized CCT of the pristine light engine using each ED subjected to 85/85 at 3154 hours.

TABLE 6. Statistical parameters for Figure 18.

Mean	1.0044706
Standard Deviation	0.0039101
Standard Error of the Mean	0.001045
Upper 95% Mean	1.0067282

TABLE 7. Statistical parameters for Figure 19.

Mean	0.0008758
Standard Deviation	0.0004311
Standard Error of the Mean	0.0001152
Upper 95% Mean	0.0011247

the mean is approximately 2000lm with a very small standard deviation of about 5.5lm. The single outlier of 2015lm is still well within the rated luminous flux value of this lighting system. All of the Quantiles are inside the Lilliefors confidence bounds and closely match the estimation of the expected mean. This demonstrates that the initial luminous flux values from both tests have no significant difference. Similarly, this is shown in the results for the initial CCT. The estimated mean of the CCT is 2732 which is about

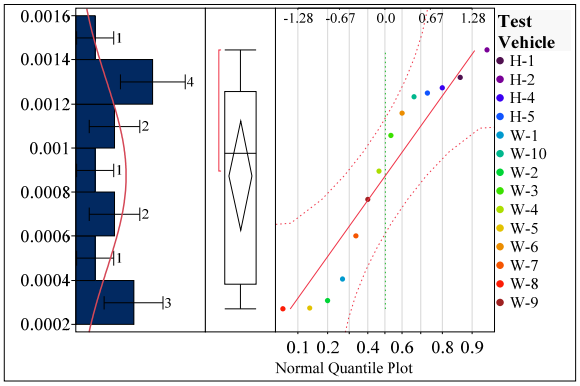

FIGURE 19. The CIE 1976 coordinate system color shift of the pristine light engine using each ED subjected to 85/85 at 3154 hours.

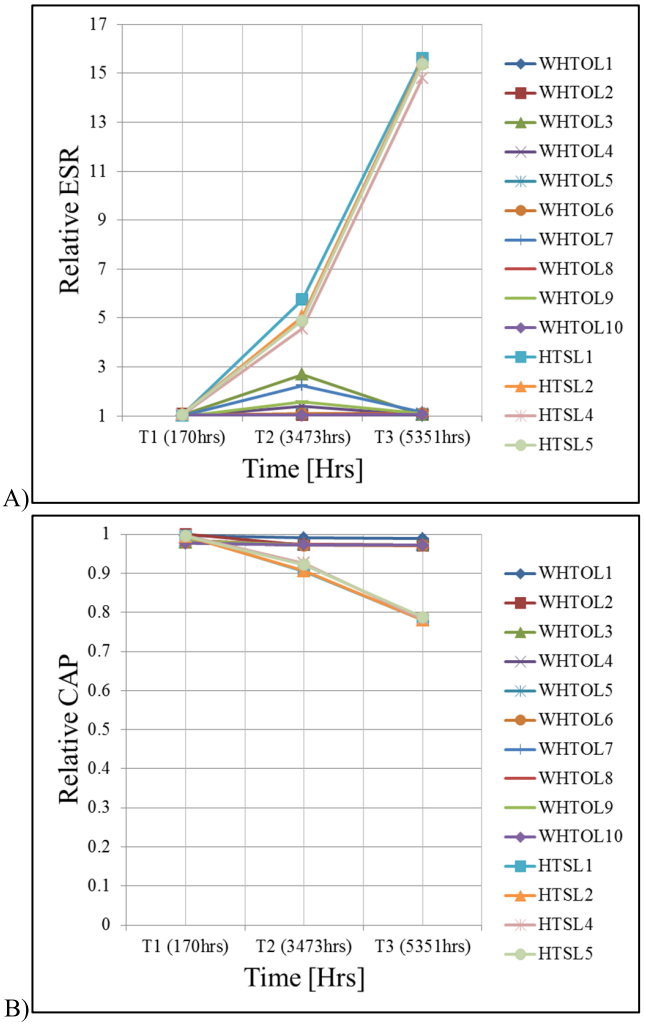

FIGURE 20. The accelerated aging comparison of AEC 1 from each ED that was subjected to 85/85 and HTSL at 170 hours, 3473 hours, and 5351 hours for relative A) CAP and B) ESR.

a 1% difference from the rated value. The Quantiles are inside the Lilliefors confidence bounds except for one value. However, all the initial CCT values are less than 2% of

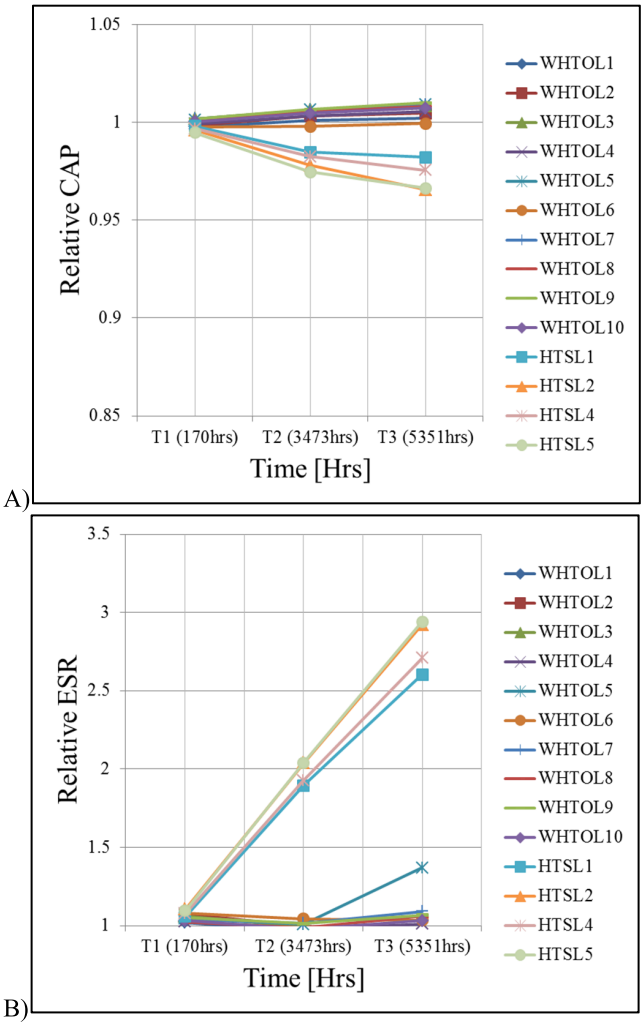

FIGURE 21. The accelerated aging comparison of AEC 2 from each ED that was subjected to 85/85 and HTSL at 170 hours, 3473 hours, and 5351 hours for relative A) CAP and B) ESR.

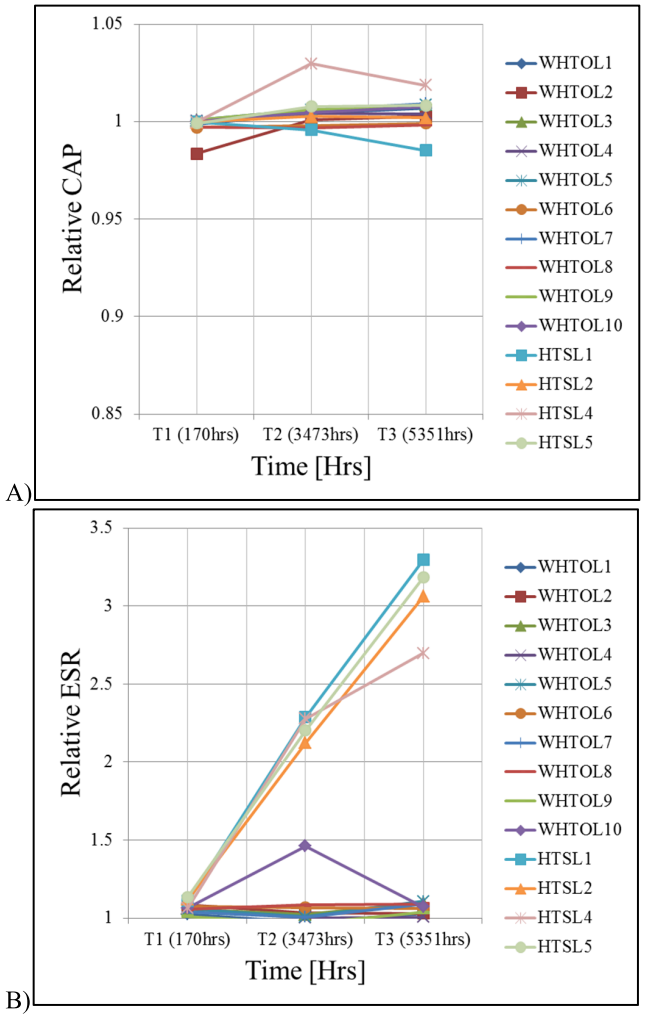

FIGURE 22. The accelerated aging comparison of AEC 3 from each ED that was subjected to 85/85 and HTSL at 170 hours, 3473 hours, and 5351 hours for relative A) CAP and B) ESR.

the rated CCT. Therefore, there is no statistical difference between the initial CCT values of both tests. From the initial values, the 85/85 and HTSL tests have no statistical differences and can, therefore, be compared. The same analysis was carried out at the same time step of 3154 hours for the normalized luminous flux, normalized CCT and color shift of the 85/85 and HTSL testing with the statistical parameters of each in Table 5, Table 6 and Table 7, respectively.

Similarly to the initial values, all of the Quantiles are inside the Lilliefors confidence bounds and closely match the estimation of the expected mean. This shows no statistical difference between the photometric quantities from the 85/85 and HTSL tests. This statistical analysis allows for the comparison of the ESR and CAP from both data sets.

HTSL testing produced wear-out failures and was beneficial in measuring the leading indicators of CAP and ESR for prognostic and health management techniques. Conversely, the 85/85 test produced catastrophic failures with no noticeable change in the hypothesized leading indicators. The comparative results of ESR and CAP for each AEC at three different measurement times is shown below.

From the relative CAP and ESR graphs located in Figures 20–23, it is quite obvious that the HTSL accelerated test had a much larger effect on the AECs performance than the 85/85 testing. The 85/85 test was used to accelerate the ingress of moisture into the AEC, as well as the EDs. Conversely, HTSL testing enhanced the degradation due to high thermal stresses. In this case, the lower temperature condition used in the 85/85 test proved too small to allow moisture to penetrate the external seals of the AECS, but did prove sufficient to accelerate the degradation of other unforeseen components inside the ED. The results demonstrate HTSL testing as a better choice to induce degradation inside the AECs for the purpose of monitoring ESR and CAP as prognostic indicators.

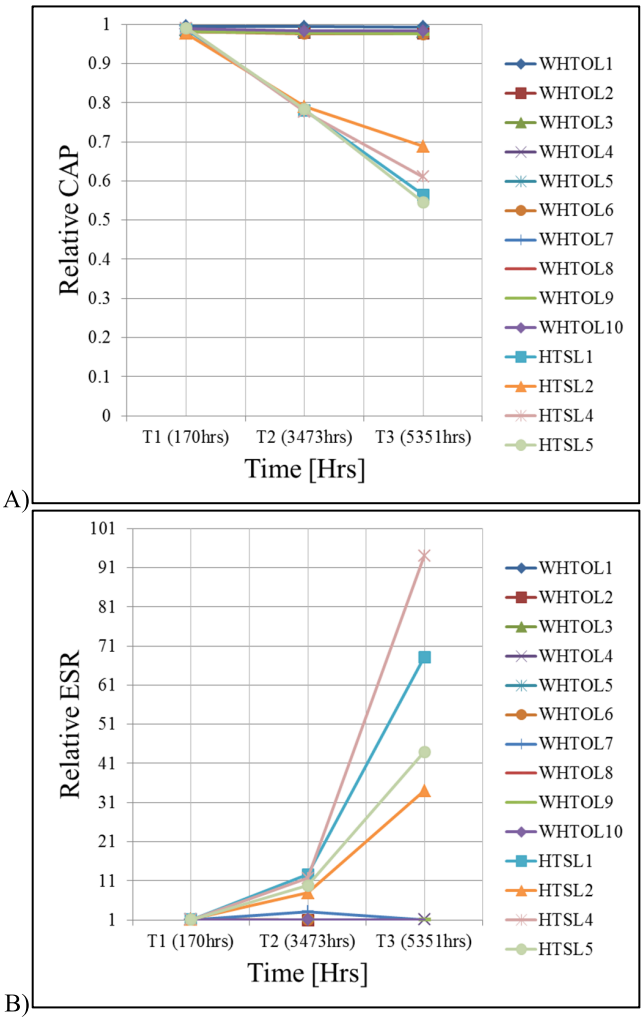

FIGURE 23. The accelerated aging comparison of AEC 4 from each ED that was subjected to 85/85 and HTSL at 170 hours, 3473 hours, and 5351 hours for relative A) CAP and B) ESR.

VII. SUMMARY & CONCLUSIONS

An investigation of an off-the-shelf device with the focus on the EDs has been demonstrated. Specific components inside the ED, the AECs, were monitored as possible precursors of failure due to previous results from HTSL testing. The EDs were aged using an accelerated life test of 85°C/85% RH. The four AECs of three different types inside each electronic driver were removed from the driver to obtain the exact CAP and ESR values using a handheld LCR meter. To monitor the overall health of the ED, the photometric quantities of a single pristine light engine was measured for each ED under test.

It was hypothesized that the AECs would be the ''weakest link'' of the electrical driver and a suitable leading indication of failure well before failure occurred. This was based off previously reported results for accelerated aging of the same test vehicle at 135°C. The measured parameters proved not to be an indication of failure for the EDs subjected to 85/85 accelerated aging. The temperature condition was much smaller than the maximum rated operating condition and did not facilitate the ingress of moisture into the AECs. The HTSL accelerated aging produced measureable degradation that is suitable for prognostic based lifetime predictions. Therefore, extreme temperature conditions will facilitate AEC degradation more rapidly than nominal temperature conditions.

The CAP, ESR and photometric quantities produced virtually constant results throughout the course of experimentation. The parameters did not give any indication the system was going to fail. There were two predominate, failure site observed during testing which comprised 70% of the test vehicles. One predominate, failure mechanism was the CL21 series polyester film capacitor located on the topside the electrical driver. This film capacitor started spewing the internal material and smoking. The electrical driver was still functional and powered the light engine normally. It was deemed failed because of health and safety concerns due to the possible toxic nature of the internal material. The other predominate, failure mechanism was an IGBT/MOSFET located on the undercarriage of the electrical driver. In this case, the top of the IGBT/MOSFET was blown off causing catastrophic failure to the system and was likely due to an electrical surge from moisture seepage into the component. Neither one of the observed, failure sites overlapped meaning each test vehicle experienced one specific failure mechanism with only two failure modes present during the 85/85 testing: an open circuit/no light and capacitance degradation.

A statistical analysis of the photometric parameters was conducted to demonstrate that the 85/85 could be compared to HTSL. This analysis showed that the initial luminous flux and CCT values had no significant difference between the two tests, as well as no significant difference between the relative luminous flux, relative CCT and color shift at 4294 hours of testing. Since there was no significant difference between the photometric quantities, the CAP and ESR values were compared for three time steps that overlapped between the two aging experiments. Based off the results, HTSL was able to produce degradation in the AECs without any premature failures to the EDs, whereas 85/85 produced sudden, catastrophic failures in the EDs and produced no discernable degradation in the AECs. In conclusion, both tests showed promising results on the reliability of the LED driver. HTSL was useful to produce degradation in the AECs for the development of reliability modeling, whereas 85/85 demonstrated the overall robustness of the ED and its susceptibility to fail due to a humid environment.

APPENDIX – NOMENCLATURE

SSL	Solid-State Lighting
LED	Light-Emitting Diode
ED	Electrical Driver
CAP	Capacitance
ESR	Equivalent Series Resistance
AEC	Aluminum Electrolytic Capacitor
LCR	Inductance, Capacitance and Resistance

85/85	85% RH & 85°C
HTSL	135°C
EISA	Energy Independence and Security Act
T_o	Operating Temperature
V_o	Operating Voltage
C_o	Operating Capacitance
$\Phi_{test}(\lambda)$	Corrected Test Lamp Spectral Radiant Flux
$\Phi_{ref}(\lambda)$	Reference (or Calibration) Lamp Spectral Radiant Flux
$y_{test}(\lambda)$	Measured Test Lamp Spectral Radiant Flux
$y_{ref}(\lambda)$	Measured Reference Lamp Spectral Radiant Flux
$\Phi_m(\lambda)$	SpectraSuite Software Spectral Radiant Flux
α_{CCF}	Absorption Correction Factor
$y_{aux,TEST}(\lambda)$	Measured Auxiliary Lamp Spectral Radiant Flux with Test Lamp
$y_{aux,REF}(\lambda)$	Measured Auxiliary Lamp Spectral Radiant Flux with Reference Lamp
Φ_{test}	Luminous Flux
$V(\lambda)$	Spectral Luminous Efficiency Function
K_m	Maximum Spectral Luminous Efficacy
k	Normalizing Factor
$\bar{x}(\lambda)$, $\bar{y}(\lambda)$, $\bar{z}(\lambda)$	CIE 1931 Standard 2° Observer Color Matching Functions
X, Y, Z	Tristimulus Values
$E(\lambda)$	Relative Spectral Power Distribution of a CIE Standard Illuminant
x, y	CIE 1931 Chromaticity Coordinates
u`, v`	CIE 1976 Chromaticity Coordinates
CCT	Correlated Color Temperature

REFERENCES

[1] *Solid-State Lighting Multi-Year Market Development Support Plan*, U.S. Department Energy, Office Energy Efficiency, Building Technologies Program, Solid-State Lighting Program, Washington, DC, USA, May 2012.

[2] *Energy Independence and Security Act of 2007*, U.S. Congress, Washington, DC, USA, Dec. 2007.

[3] *LED Luminaire Lifetime: Recommendations for Testing and Reporting*, 2nd ed., Next Generation Lighting Industry Alliance and U.S. Department of Energy, Washington, DC, USA, Jun. 2011.

[4] M.-H. Chang, D. Das, P. V. Varde, and M. Pecht, "Light emitting diodes reliability review," *Microelectron. Rel.*, vol. 52, no. 5, pp. 762–782, 2012.

[5] P. Lall, P. Sakalaukus, and L. Davis, "Prognostics of damage accrual in SSL luminaires and drivers subjected to HTSL accelerated aging," in *Proc. ASME Int. Tech. Conf. Exhibit. Packag. Integr. Electron. Photon. Microsyst.*, 2013, pp. V001T04A018-1–V001T04A018-8.

[6] P. Lall, H. Zhang, and L. Davis, "Assessment of lumen degradation and remaining life of LEDs using particle filter," in *Proc. ASME Int. Tech. Conf. Exhibit. Packag. Integr. Electron. Photon. Microsyst.*, 2013, pp. V001T04A024-1–V001T04A024-13.

[7] N. Narendran, Y. Gu, J. P. Freyssinier, H. Yu, and L. Deng, "Solid-state lighting: Failure analysis of white LEDs," *J. Crystal Growth*, vol. 268, nos. 3–4, pp. 449–456, 2004.

[8] R. Baillot *et al.*, "Effects of silicone coating degradation on GaN MQW LEDs performances using physical and chemical analyses," *Microelectron. Rel.*, vol. 50, nos. 9–11, pp. 1568–1573, 2010.

[9] P. McCluskey, K. Mensah, C. O'Connor, F. Lilie, A. Gallo, and J. Fink, "Reliability of commercial plastic encapsulated microelectronics at temperatures from 125 °C to 300 °C," in *Proc. IEEE Aerosp. Conf.*, Big Sky, MT, USA, Mar. 2000, pp. 445–450.

[10] P. McCluskey, K. Mensah, C. O'Connor, and A. Gallo, "Reliable use of commercial technology in high temperature environments," *Microelectron. Rel.*, vol. 40, nos. 8–10, pp. 1671–1678, 2000.

[11] M. Meneghini, L.-R. Trevisanello, G. Meneghesso, and E. Zanoni, "A review on the reliability of GaN-based LEDs," *IEEE Trans. Device Mater. Rel.*, vol. 8, no. 2, pp. 323–331, Jun. 2008.

[12] *Luxeon Reliability Datasheet RD25*, Philips Lumileds Lighting Company, San Jose, CA, USA, 2006.

[13] X. Luo, B. Wu, and S. Liu, "Effects of moist environments on LED module reliability," *IEEE Trans. Device Mater. Rel.*, vol. 10, no. 2, pp. 182–186, Jun. 2010.

[14] Y.-C. Hsu *et al.*, "Failure mechanisms associated with lens shape of high-power LED modules in aging test," *IEEE Trans. Electron Devices*, vol. 55, no. 2, pp. 689–694, Feb. 2008.

[15] *Reliability of Precision Optical Performance AllnGaP LED Lamps in Traffic Signals and Variable Message Signs*, Hewlett Packard, Palo Alto, CA, USA, 1997.

[16] R.-J. Xie and N. Hirosaki, "Silicon-based oxynitride and nitride phosphors for white LEDs—A review," *Sci. Technol. Adv. Mater.*, vol. 8, nos. 7–8, pp. 588–600, 2007.

[17] C. S. Kulkarni, J. R. Celaya, K. Goebel, and G. Biswas, "Physics based electrolytic capacitor degradation models for prognostic studies under thermal overstress," in *Proc. 1st Eur. Conf. Prognostics Health Manage. Soc.*, Dresden, Germany, 2012, pp. 156–164.

[18] A. M. Imam, T. G. Habetler, R. G. Harley, and D. M. Divan, "Condition monitoring of electrolytic capacitor in power electronic circuits using adaptive filter modeling," in *Proc. IEEE 36th Power Electron. Specialists Conf. (PESC)*, Recife, Brazil, Jun. 2005, pp. 601–607.

[19] C. S. Kulkarni, J. R. Celaya, G. Biswas, and K. Goebel, "Accelerated aging experiments for capacitor health monitoring and prognostics," in *Proc. IEEE AUTOTESTCON*, Anaheim, CA, USA, Sep. 2012, pp. 356–361.

[20] S. Lan, C. M. Tan, and K. Wu, "Reliability study of LED driver—A case study of black box testing," *Microelectron. Rel.*, vol. 52, nos. 9–10, pp. 1940–1944, 2012.

[21] A. M. Georgiev, *The Electrolytic Capacitor*. New York, NY, USA: Murray Hill Books, 1945.

[22] *Technical Notes for Electrolytic Capacitor*, Rubycon Corp., Nagano, Japan, 2013.

[23] *General Descriptions of Aluminum Electrolytic Capacitors*, Nichicon Inc., Kyoto, Japan, 2002.

[24] A. Albertsen, *Electrolytic Capacitor Lifetime Estimation*, Jianghai Eur. GmbH, Krefeld, Germany, 2010.

[25] L. Han and N. Narendran, "Developing an accelerated life test method for LED drivers," *Proc. SPIE*, vol. 7422, p. 742209, Aug. 2009.

[26] K. Harada, A. Katsuki, and M. Fujiwara, "Use of ESR for deterioration diagnosis of electrolytic capacitor," *IEEE Trans. Power Electron.*, vol. 8, no. 4, pp. 355–361, Oct. 1993.

[27] M. L. Gasperi, "Life prediction model for aluminum electrolytic capacitors," in *Proc. Conf. Rec. IEEE Ind. Appl. Soc.*, vol. 3. Oct. 1996, pp. 1347–1351.

[28] *Aluminum Electrolytic Capacitor Application Notes*, BHC Components, Dorset, U.K., 2002.

[29] V. A. Sankaran, F. L. Rees, and C. S. Avant, "Electrolytic capacitor life testing and prediction," in *Proc. IEEE Ind. Appl. Conf.*, vol. 2. Oct. 1997, pp. 1058–1065.

[30] J. L. Stevens, J. S. Shaffer, and J. T. Vandenham, "The service life of large aluminum electrolytic capacitors: Effects of construction and application," in *Proc. IEEE Ind. Appl. Conf.*, Sep./Oct. 2002, pp. 2493–2499.

[31] *Aluminum Electrolytic Capacitors*, Panasonic Industrial Company, Newark, NJ, USA, 2008.

[32] *Application Guide, Aluminum Electrolytic Capacitors*, Cornell Dubilier Electronics Inc., Liberty, SC, USA, 2000.

[33] J. Celaya, C. Kulkarni, G. Biswas, S. Saha, and K. Goebel, "A model-based prognostics methodology for electrolytic capacitors based on electrical overstress accelerated aging," in *Proc. Annu. Conf. Prognostics Health Manage. Soc.*, Montreal, QC, Canada, Sep. 2011, pp. 31–39.

[34] *JEDEC Steady State Temperature Humidity Bias Life Test Standard*, document JESD22-A101C, 2009.

[35] *Approved Method: Electrical and Photometric Measurements of Solid-State Lighting Products*, IES Standards LM-79–08, 2008.

[36] C. DeCusatis, Ed., *Handbook of Applied Photometry*. New York, NY, USA: AIP Press, 1997.
[37] J. Schanda, Ed., *Colorimetry: Understanding the CIE System*. Hoboken, NJ, USA: Wiley, 2007.
[38] S. Westland and C. Ripamonti, *Computational Colour Science Using MATLAB*. Hoboken, NJ, USA: Wiley, 2004.
[39] Y.-F. Hsieh, M. Ou-Yang, T.-W. Huang, and C.-C. Lee, "Determination of optimal converting point of color temperature conversion complied with ANSI C78. 377 for indoor solid-state lighting and display applications," *Opt. Exp.*, vol. 20, no. 18, pp. 20059–20070, Aug. 2012.
[40] J. Hernández-Andrés, R. L. Lee, Jr., and J. Romero, "Calculating correlated color temperatures across the entire gamut of daylight and skylight chromaticities," *Appl. Opt.*, vol. 38, no. 27, pp. 5703–5709, Sep. 1999.
[41] P. Lall, P. Sakalaukus, and L. Davis, "Reliability of solid-state lighting electrical drivers subjected to WHTOL accelerated aging," in *Proc. IEEE Intersoc. Conf. Thermal Thermomech. Phenomena Electron. Syst. (ITherm)*, Lake Buena Vista, FL, USA, May 2014, pp. 1164–1170.
[42] *JEDEC High Temperature Storage Life Standard*, document JESD22-A103D, 2010.

PRADEEP LALL (M'93–SM'08–F'12) received the B.E. degree in mechanical engineering from the Delhi College of Engineering, Delhi, India, in 1988, the M.S. and Ph.D. degrees in mechanical engineering from the University of Maryland, College Park, MD, USA, in 1989 and 1993, respectively, and the M.B.A. degree from the Kellogg School of Management, Northwestern University, Evanston, IL, USA, in 2002. He is currently the John and Anne MacFarlane Professor with the Department of Mechanical Engineering, and the Director of the NSF Center for Advanced Vehicle and Extreme Environment Electronics, Auburn University.

He was with the Motorola's Wireless Technology Center. He has published extensively in the area of electronic packaging with an emphasis on modeling and predictive techniques. He has authored or co-authored two books, 14 book chapters, and over 400 journal and conference papers in the field of electronic packaging with an emphasis on design, modeling, and predictive techniques. He is a fellow of the American Society of Mechanical Engineers, and the Alabama Academy of Science.

Dr. Lall holds three U.S. Patents. He was a recipient of the IEEE Exceptional Technical Achievement Award, the ASME's Applied Mechanics Award, the SMTA's Member of Technical Distinction Award, the Auburn University's Creative Research and Scholarship Award, the SEC Faculty Achievement Award, the Samuel Ginn College of Engineering Senior Faculty Research Award, Three-Motorola Outstanding Innovation Awards, Five-Motorola Engineering Awards, and Twenty best paper awards at national and international conferences. He has served in several distinguished roles at national and international level, including a member of the National Academies Committee on Electronic Vehicle Controls and the IEEE Reliability Society AdCom, the IEEE Reliability Society Representative on the IEEE-USA Government Relations Council for Research and Development Policy, the Chair of the Congress Steering Committee for the ASME Congress, a Member of the Technical Committee of the European Simulation Conference EuroSIME, and an Associate Editor of the IEEE Transactions on Components and Packaging Technologies. He is a Six-Sigma Black-Belt in Statistics. He is the Founding Faculty Advisor of the SMTA Student Chapter at Auburn University, and a member of the Editorial Advisory Board of the *Journal of Surface Mount Technology*.

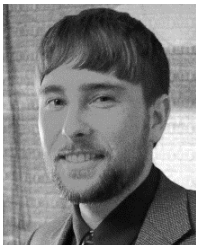

PETER SAKALAUKUS (M'12) received the B.S. degree in mechanical engineering from Mississippi State University, Starkville, MS, USA, in 2006, and the M.S. degree in mechanical engineering from the University of South Alabama, Mobile, AL, USA, in 2011. He is currently pursuing the Ph.D. degree in mechanical engineering with Auburn University, Auburn, AL, USA.

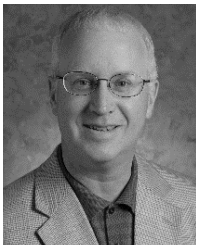

LYNN DAVIS is currently the Director of the Nanoenabled Devices Program with RTI International. He serves as a Principal Investigator and the Chief Inventor of RTI's Nanofiber Lighting Improvement Technology (NLITe) for use in high-efficiency general illumination. NLITe has been recognized with several national and international awards, including the Research and Development 100 Award from *Research and Development Magazine*, the FM100 Award from *Future Materials Magazine*, the Innovation Award from the Energy Institute, and was voted as a Finalist for the World Technology Award for Materials.

He received the 1906 Award from the International Electrotechnical Commission (IEC) for developing the first electrotechnical product-oriented IEC standard in nanotechnology. He led an international team of experts from IEC to draft, research, and create the standard to determine the efficiency of luminescent nanomaterials used in lighting and display products.